Bioconjugate Chemistry

Subscriber access provided by University of South Dakota

Article

Ultrasound-Responsive Nanoparticulate for Selective Amplification of Chemotherapeutic Potency for Ablation of Solid Tumors

Jing Xia, Jingyun Wang, Xiang Wang, Ming Qian, Liuwei Zhang, and Qixian Chen

Bioconjugate Chem., **Just Accepted Manuscript** • DOI: 10.1021/acs.bioconjchem.8b00626 • Publication Date (Web): 06 Sep 2018

Downloaded from http://pubs.acs.org on September 6, 2018

Just Accepted

"Just Accepted" manuscripts have been peer-reviewed and accepted for publication. They are posted online prior to technical editing, formatting for publication and author proofing. The American Chemical Society provides "Just Accepted" as a service to the research community to expedite the dissemination of scientific material as soon as possible after acceptance. "Just Accepted" manuscripts appear in full in PDF format accompanied by an HTML abstract. "Just Accepted" manuscripts have been fully peer reviewed, but should not be considered the official version of record. They are citable by the Digital Object Identifier (DOI®). "Just Accepted" is an optional service offered to authors. Therefore, the "Just Accepted" Web site may not include all articles that will be published in the journal. After a manuscript is technically edited and formatted, it will be removed from the "Just Accepted" Web site and published as an ASAP article. Note that technical editing may introduce minor changes to the manuscript text and/or graphics which could affect content, and all legal disclaimers and ethical guidelines that apply to the journal pertain. ACS cannot be held responsible for errors or consequences arising from the use of information contained in these "Just Accepted" manuscripts.

ACS Publications

is published by the American Chemical Society. 1155 Sixteenth Street N.W., Washington, DC 20036

Published by American Chemical Society. Copyright © American Chemical Society. However, no copyright claim is made to original U.S. Government works, or works produced by employees of any Commonwealth realm Crown government in the course of their duties.

Ultrasound-Responsive Nanoparticulate for Selective Amplification of Chemotherapeutic Potency for Ablation of Solid Tumors

Jing Xia,[†‡] Jinyun Wang,[†‡] Xiang Wang,[‡] Ming Qian,[‡] Liuwei Zhang,[‡] Qixian Chen[†‡*]

[†]State Key Laboratory of Fine Chemicals, Dalian University of Technology, No. 2 Linggong Road, Dalian 116024, China

[‡]School of Life Science and Biotechnology, Dalian University of Technology, No. 2 Linggong Road, Dalian 116024, China

*All correspondence should be addressed to Q. C. (E-mail: qixian@dlut.edu.cn).

ABSTRACT: Precision medicine requests preferential transportation of the pharmaceutical substances to the pathological site and impartation of localized therapeutic activities to the targeted cells. To accomplish this goal, we attempted a facile nanoscaled ultrasound-responsive delivery system, characterized by doxorubicin assembled with an amphiphilic copolymer (multiple of hydrophobic stearic segments tethered onto the hydrophilic pullulan backbone through ultrasound-labile oxyl-alkylhydroxylamine linkage). As a consequence of the strategically installed ultrasound-labile oxyl-alkylhydroxylamine linkage to elicit the tailored segregation of the hydrophilic pullulan and the hydrophobic stearic segments upon ultrasound impetus, the constructed nanoscaled self-assembly presented distinctive structural destabilization behaviors and afforded spatiotemporal controlled liberation of the cytotoxic drugs. It is worthy to note that the ultrasound was determined to markedly lower the IC_{50} of the proposed system from over 10 μg/mL to 2.33 μg/mL (approximate 4-fold), thereby serving as a facile impetus to amplify the cytotoxic potency of the proposed drug delivery vehicles. Furthermore, drastic tumor ablation was validated by dosage of the proposed doxorubicin delivery system to T41 tumor-bearing mice in accompanied with the tumor-localized ultrasound impetus, while no observable adverse side effect was confirmed. Therefore, the results advocated our ultrasound-responsive delivery vehicle as a tempting strategy for precise spatiotemporal control of the release of the drug cargos, thus affording selectively amplified cytotoxic potency to the ultrasound-imposed site, which should be highlighted as an important progress toward precision medicine.

KEYWORDS: *pullulan, ultrasound-responsive, tumor therapy, drug delivery, doxorubicin*

INTRODUCTION

The development of nanotechnology has led to appreciation of nanoparticulate-based delivery strategies, termed as nanomedicine, to be capable of affording targeted transportation of therapeutic substances to the pathological sites. Particularly, the chemotherapeutic drugs, once encapsulated into appropriate targeted delivery vehicles, are postulated to remarkably improve the drug availabilities to the pathological tissues, consequently conducing to improved therapeutic potency and reduced off-target adverse effect [1-3]. To date, a number of nanoparticulates encapsulating chemotherapeutic drugs were approved by FDA for treatment of intractable cancers, including Doxil, DaunoXome, Mariqbo, Lipusu and Abraxane [2, 4-5]. These drug formulations were documented to exert appreciable tumor-preferential accumulation activities either by passive targeting approach based on the tumor-characterized enhanced permeability and retention (EPR) properties [6-7] or active targeting strategies with aids of specific antibodies or ligands [8-9]. Nevertheless, in subsequence to tumor accumulation, the drug release kinetics from the delivery nanoparticulates usually relied on the slow drug diffusion rate or the chronic degradation process of the delivery materials, which substantially restricted the subsequent therapeutic potency [10-11]. Spatiotemporal control of drug release at the targeted location is imperative to advance nanomedicine towards practical applications. Aiming to promote the therapeutic efficacy at the targeted site, a number of stimuli-responsive facilities was devised into the delivery nanoparticulates [12-13] to pursue accelerated drug release at the tumor sites in response to endogenous stimuli (i.e., pH, glutathione, hypoxia, enzymes and other tumor markers) [14-18] or exogenous stimuli (i.e., temperature, electromagnetic radiation and particle radiation) [6, 19-20].

In view of a variety of stimuli, ultrasound is deemed to be an attractive impetus to seek targeted amplification of therapeutic efficacy of the nanomedicine with respect to its inherent advantages of precise spatiotemporal controllability, noninvasiveness and excellent tissue penetration depth [21-23].

As opposed to the other exogenous stimulus (ionizing electromagnetic radiation, particle radiation, electric impulse, etc.), the remarkable safety profile of ultrasound to the human body led to appreciation of ultrasound as a tempting external impetus. Moreover, the high-frequency ultrasound to elicit deep tissue penetration is envisioned to render a burst drug release and subsequent potent cytotoxicity selectively to the ultrasound-localized tumors, thereby minimizing the adverse side effects to the off-target tissues. Moreover, ultrasound stimuli also appeared to be beneficial in promoting nanoparticle extravasation through blood capillaries and nanoparticle permeation across cell membrane[24-26]. Therefore, ultrasound represented an intriguing alternative stimulus to trigger the precise controlled drug release at the desired site in a spatially and temporally manner, with the ultimate aim of improved therapeutic efficacy and minimized adverse effects. Note that the pioneer research from Dr. J. L. Paris et al.[26] has developed a novel ultrasound-responsive doxorubicin (DOX) delivery formation based on mesoporous silica nanoparticles grafted with copolymers containing ultrasound-labile chemical bonds on their surface that served as gatekeeper of the silica pores. Upon ultrasound impetus, the ultrasound-responsive system was subjected to marked molecular transformation to induce the emergence of abundant avenues and facilitate the release of the DOX payloads.

In the present study, we attempted to synthesize a novel pullulan-based drug delivery system, self-assembled from amphiphilic copolymer with hydrophobic doxorubicin payloads. Particularly, the pullulan-based amphiphilic polymer was characterized to have a pullulan (referred as P in the abbreviation of amphiphilic polymer) backbone tethered with a multiple of hydrophobic stearic (SC) segments through ultrasound-labile linkage of oxyl-alkylhydroxylamine bond (-*oa*-) (P-*oa*-SC in Scheme 1). Noteworthy is pullulan produced by aureobasidium pullulans, which is a homopolysaccharide consisting of maltotriose units. Due to its excellent biocompatibility and modifiability, pullulan has been widely employed in biomedical applications[27-29]. As shown in Scheme 1 (Figure 1), DOX as a hydrophobic anticancer drug was chosen as a model drug and successfully

loaded into the P-*oa*-SC self-assembly formation. The obtained pullulan-based ultrasound-triggered DOX delivery system (P-*oa*-SC/DOX) is speculated to be capable of employing spatial-controlled ultrasound impetus to pursue precise amplification of the cytotoxic potency to the tumors, thereby entitling selectively enhancement of anti-tumor efficacy to the ultrasound-specified tumor site due to the ultrasound-mediate accelerated drug release and minimal toxicity to the normal tissue due to the reluctant drug release.

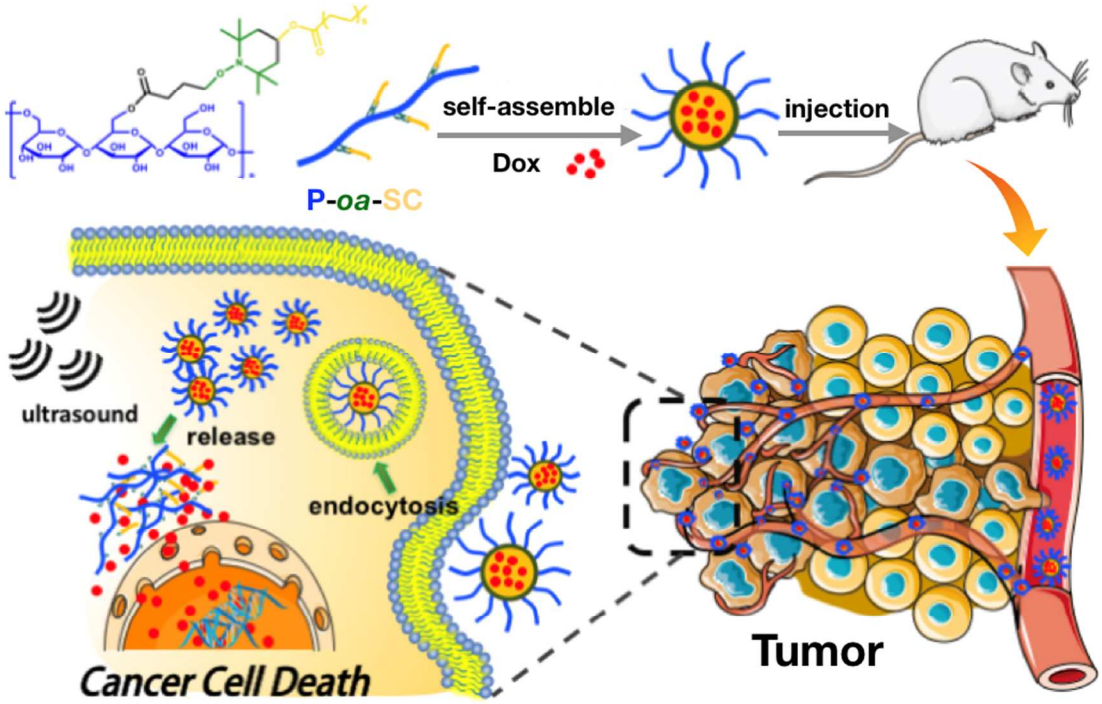

Scheme 1. Illustration of construction of ultrasound-responsive P-*oa*-SC/DOX nanoparticulates to pursue ultrasound-specified chemotherapeutic potency to the tumors.

RESULTS AND DISCUSSION

Polymer Synthesis and Characterizations. The amphiphilic copolymer of P-*oa*-SC was synthesized according to the synthetic scheme (Figure 1a). In brief, the precursor pullulan bearing a variety of chlorides was obtained through acylation reaction between the acryl chloride group of 4-chlorobutyryl chloride and the hydroxyl groups of pullulans. On the other hand,

4-hydroxyl-2,2,6,6-tetramethyl-1-piperidine oxidanyl radical (HTEMPO) was introduced to the acryl chloride group of stearic chloride through acylation reaction to yield nitroxide radical functionalized stearic derivative (OC). The above yielded products were linked based on nitroxide radical coupling reaction between chlorinated pullulan (P-Cl) and OC to yield P-*oa*-SC, wherein the -*oa*- linkage served as a facile ultrasound-labile linkage.

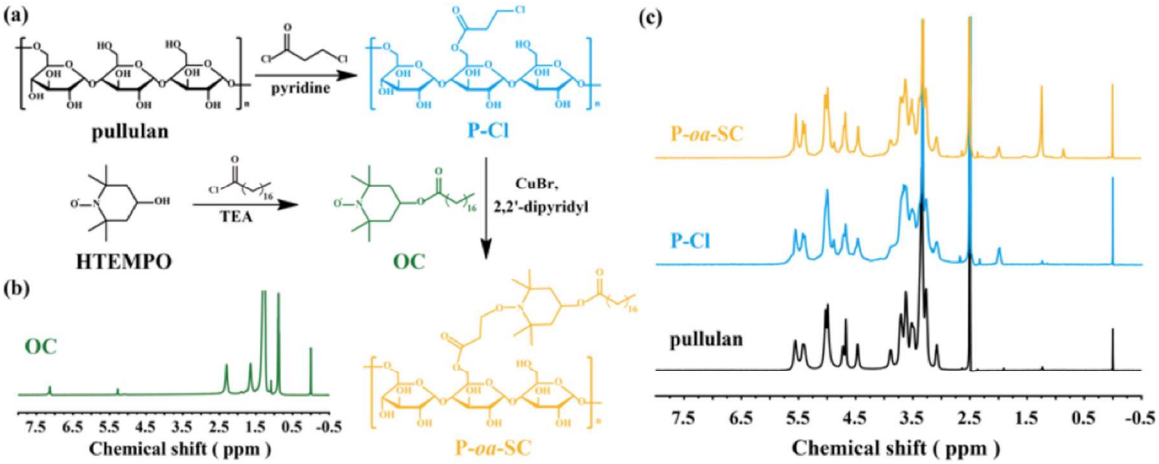

Figure 1. Synthetic scheme and characterizations of P-*oa*-SC. (a): synthetic scheme of P-*oa*-SC; (b): ^{1}H-NMR spectrum of OC in $CDCl_3$; (c) ^{1}H-NMR spectra of pullulan and its derivatives in DMSO-$_6$.

The yielded products of OC, P-Cl and P-*oa*-SC were characterized by ^{1}H-NMR measurement. The representative spectra of OC in $CDCl_3$ was shown in Figure 1b, wherein the peaks at 5.23 ppm and 1.26 ppm could be assigned to the methine (-CH-O) and methyl (-CH_3) moieties of piperidine and the peak at 0.88 ppm corresponding to the methyl (CH_3) moiety of stearic acid. The ^{1}H-NMR results verified the successfully synthesis of OC. On the other hand, the ^{1}H-NMR spectrum of pullulan and its derivatives was shown in Figure 1c. Note that the broad peak in the range of 3.0–4.0 ppm could be assigned to the methine and methylene protons (CH-O and CH_2-O) of pullulan [17] while the doublet at approximate 5.5 ppm corresponds to the methylidyne proton (O-CH-O) on glucose units of pullulan[30] and the peak at 1.96 ppm belongs to methylene (-CO-CH_2-CH_2-Cl) of chlorobutyryl chloride. The

peaks at 0.85 ppm and 1.23 ppm could be assigned to the methyl (-CH_3) and methylene (-CH_2) on alkyl segment of stearic chloride. Overall, the number of chlorides in P-Cl was determined to be approximate 7.21 per 100 glucose units and approximate 4.2 SC segments per 100 glucose units.

To test the feasibility of -*oa*-cleavage in P-*oa*-SC responsive to ultrasound impetus, the P-*oa*-SC solution was subjected to ultrasound treatment for 5 min, and the reaction solution was transferred to liquid chromatography and mass spectrometry measurements. As shown in Figure 2b, distinctive stearic derivative was observed in liquid chromatography (resembling the liquid chromatography trace of the reference stearic acid). Moreover, mass spectrometry characterization for the product of Figure 2b(v) affirmed its molecular weight to be approximate 440.4 Da, indicating the production of stearic alcohol [as shown in the chemical structure of Figure 2b(iv)]. These results validated our strategically engineering ultrasound-specific labile -*oa*- linkage to attain ultrasound-mediated segregation of hydrophilic pullulan and hydrophobic stearic derivatives.

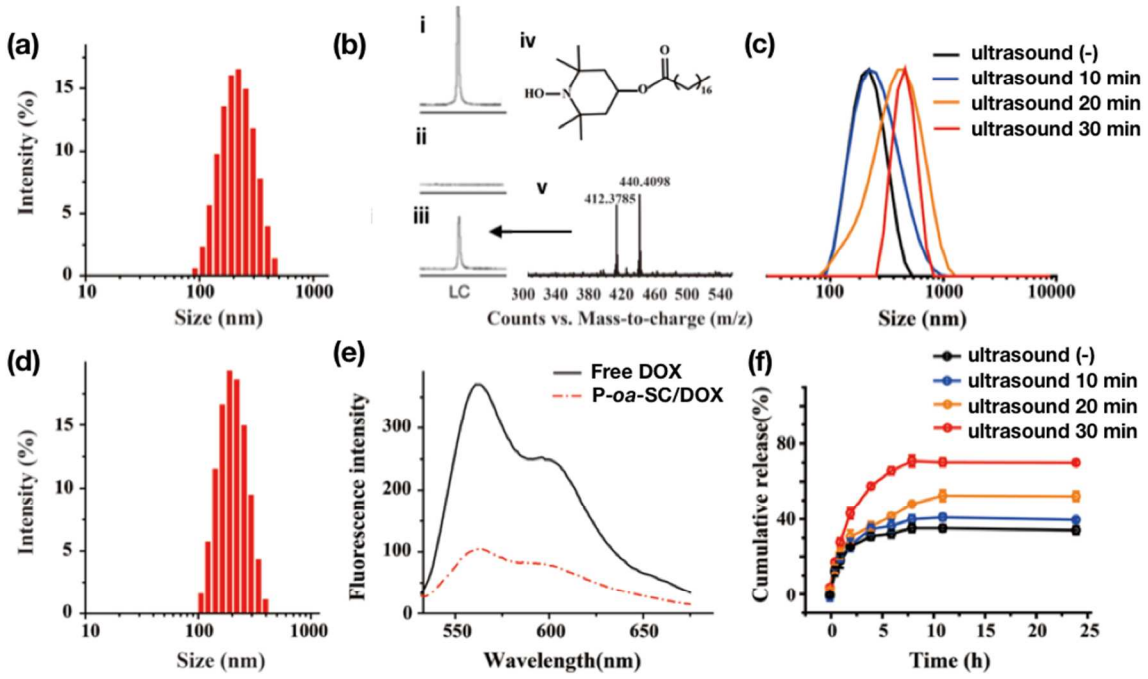

Figure 2. Characterizations of P-*oa*-SC and P-*oa*-SC/DOX. (a): DLS measurement for the P-*oa*-SC self-assembly; (b) cleavage of -*oa*- linkage in P-*oa*-SC responsive to ultrasound impetus, the liquid

chromatography of the reference OC (i), P-*oα*-SC in absence of ultrasound impetus (ii) P-*oα*-SC in presence of ultrasound impetus (iii), iv): the inferred chemical structure of OC derivatives as the product of the ultrasound-mediated P-*oα*-SC cleavage, v): the mass spectrometry of the peak fraction in LC iii); (c): DLS measurement for the P-*oα*-SC self-assembly upon ultrasonication (1.0 MHz, 9.9 W, 3 W/cm^2); (d): DLS measurement for P-*oα*-SC/DOX self-assembly; (e): the fluorescence emission spectra of free DOX and P-*oα*-SC/DOX; (f): the cumulative release of DOX from P-*oα*-SC/DOX in presence of ultrasound impetus (1.0 MHz, 9.9 W, 3 W/cm^2). Data were presented as means ± standard deviation (S.D.).

Ultrasound-Stimulated Destabilization of Self-Assembled Nanostructure and Its Implications in Ultrasound-Stimulated Drug Release. The ultrasound-responsive P-*oα*-SC nanoparticulates were prepared by spontaneous self-assembly of amphiphilic P-*oα*-SC by a dialysis approach, wherein the nanoscaled formation was achieved as a consequence of hydrophobic interactions between the tethered SC segments. Of note, the critical micelle concentration (CMC) of P-*oα*-SC was determined to be rather low, approximate 32 mg/L based on a pyrene assay (Figure S1). This result indicates the appreciable colloidal stabilities of P-*oα*-SC-formulated structure despite in a diluted milieu (e.g. blood circulation), which is believed to be capable of withstanding premature dissociation and release of drug payloads post administration. Herein, the self-assembled structure of P-*oα*-SC was prepared at a uniform concentration of 5 mg/mL in this study. Its formation was characterized by DLS measurement, which exhibited an approximate 202.43 ± 3.37 nm hydrodynamic diameter with unimodal distribution (PDI: approximate 0.1). Moreover, TEM measurement confirmed the formation of uniform spherical nanoparticulates (Figure S2, left image). Note that appreciable colloidal stability of the P-*oα*-SC self-assembly formation was confirmed, as evidenced by constant DLS size over 15 days incubation in PBS (Figure S3).

As validated above, the tethered stearic segments appeared to be readily detached from the pullulan due to facile -*oa*- linkage breakage upon ultrasound impetus. To explore the impact of the hydrophobic stearic segment detachment on the structure of P-*oa*-SC self-assembly, the structural destabilization of P-*oa*-SC in responsive to ultrasound impetus was studied by DLS measurement. Herein, the ultrasound (1.0 MHz, 9.9 W, 3 W/cm^2) was adopted as the impetus, which has been verified as a safety level to the biological species and the biological structures. The average DLS size of P-*oa*-SC formation was observed to follow a consistent rise from 202.80 nm to 633.30 nm with extended ultrasound treatment until 30 min. In consistent with DLS measurement, apparent structural transformation and secondary aggregation was observed for P-*oa*-SC self-assembly after ultrasonication (Figure S2, right). A plausible reason for this observation should be attributable to the ultrasound-mediated dePEGylation due to cleavage of the -*oa*- linkage, thereby resulting into the rearrangement of the self-assembled structure from amphiphilic polymers post the detachment of hydrophobic segments and aggregative reactions between the dePEGylated self-assemblies. On the contrary, the DLS size of P-*oa*-SC nanoparticulates appeared to remain constant without ultrasound despite extended incubation in PBS (10 mM) (Figure S3). Moreover, appreciable resistance of P-SC (lack of -*oa*- linkage) to ultrasound treatment was confirmed (Figure S4), implying the critical role of -*oa*- linkage in eliciting structural destabilization rather than the consequences of the mechanical turbulence of the ultrasonication[31]. Most likely, the growth in the particle size is conjectured to be as a result of the breakage of -*oa*- linkage in P-*oa*-SC. This breakage could elicit detachment of hydrophilic pullulan and hydrophobic stearic segments, thereby leading to slough-off of the hydrophilic pullulan from the tethered hydrophobic stearic segments-formulated nanostructures, ultimately accounting for structural rearrangement (e.g. secondary aggregation of the nanostructures). Hence, the results approved the utility of the ultrasound-responsive chemistry for pursuit of ultrasound-specified structural transformation of self-assembled nanoscaled delivery systems.

Furthermore, the hydrophobic drug of DOX was utilized to assemble with P-*oa*-SC with the aim of exploring the utility of the ultrasound-specified structural transformation of P-*oa*-SC self-assembly in seeking the controlled drug release functionality. Given that DOX is characterized to be an aggregation-induced quench fluorophore whose fluorescence emission was subjected to markedly drop when entrapped in an aggregated condition. Herein, the fluorescence emission spectra of DOX were used to explore the evidence of DOX entrapment into the hydrophobic stearic region of P-*oa*-SC self-assembly. As shown in Figure 2e, the DOX characteristic fluorescence emission of P-*oa*-SC/DOX appeared to be subjected to drastically drop as compared to the free DOX. A plausible reason for this aggregation-induced quench of DOX molecules should ascribe to the molecular aggregation of DOX and hydrophobic stearic segments, thereby rendering an aggregation-induced quench behavior. This result verified the facile encapsulation of DOX into the self-assembly of P-*oa*-SC structure.

The DOX release profiles from P-*oa*-SC/DOX were characterized in presence and absence of ultrasound impetus. As shown in Figure 2f, reluctant drug release was confirmed for P-*oa*-SC/DOX in absence of ultrasound impetus, approximate 35 % was determined to release at 24 h. On the contrary, ultrasound impetus appeared to markedly accelerate the drug release rate, approximate 32 % release within 1 h in presence of ultrasound treatment (1.0 MHz, 9.9 W, 3 W/cm^2, 30 min). A plausible reason for this accelerated drug release should be as a consequence of ultrasound-induced cleavage of the -*oa*- linkage. This ultrasound-triggered cleavage is speculated to prompt the detachment of the hydrophobic stearic segments and hydrophilic pullulan backbone, consequently accounting for rearrangement of the self-assembled P-*oa*-SC/DOX architecture. The structural rearrangement, together with the mechanical impact imposed by ultrasound, could facilitate the liberation of the DOX payload apart from the self-assembly. To this end, the proposed ultrasound-stimulated cleavage strategy has been validated as a feasible approach to render

ultrasound-dictating drug release functionality, which is envisioned to afford selective ultrasound-dictating cytotoxic potency to the ultrasound-imposed cells.

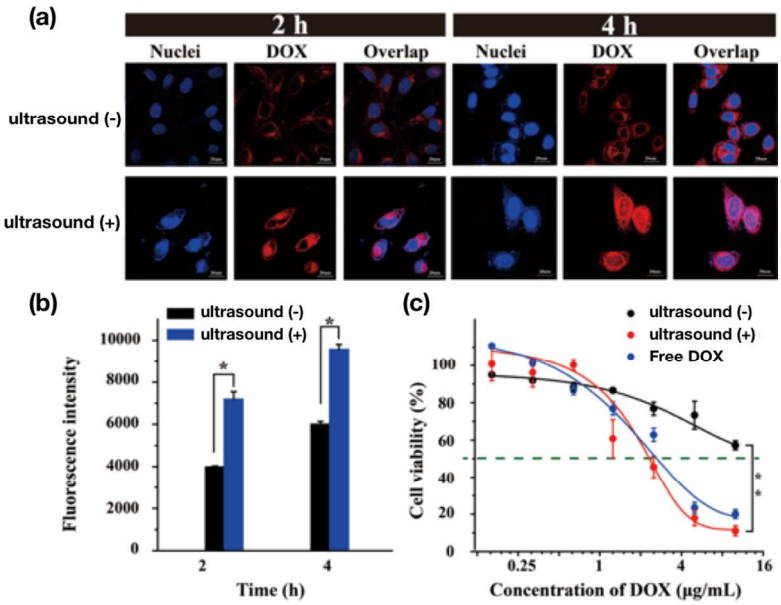

Figure 3. *In vitro* insight into the ultrasound-stimulated drug release and its impact on the cytotoxic profiles. (a): intracellular distributions of P-*oa*-SC/DOX in absence and presence of ultrasound impetus by CLSM observation; (b): quantification of intracellular fluorescence intensity of DOX for MCF-7 cells treated with P-*oa*-SC/DOX in absence or presence of ultrasound impetus(1.0 MHz, 9 W, 3 W/cm^2, 5 min); (c): cytotoxicity of P-*oa*-SC/DOX in presence or absence of ultrasound impetus (1.0 MHz, 9 W, 3 W/cm^2, 5 min) in Hep-G2 cells. Data were presented as means ± standard deviation (S.D.). $^*p < 0.05$.

Controlled Intracellular Drug Release and Nucleus-Translocation of Doxorubicin in Responsive to Ultrasound for Selective Cytotoxicity. Given that the fluorescence intensity of DOX is subject to a pronounced jump once liberated as the free molecule (Figure 2e), the intracellular fluorescence intensity of DOX was measured for the cells containing an identical amount of P-*oa*-SC/DOX in presence or absence of ultrasound impetus by flow cytometry with aim of exploring the evidence of the accelerated drug release by ultrasonication. Herein, two identical dishes of MCF-7 cells

containing a same amount of P-*oα*-SC/DOX was achieved by incubation at a same concentration of P-*oα*-SC/DOX (DOX concentration: 10 μg/mL). At 3 h post incubation, the cells were washed by PBS and immersed in fresh medium, followed by ultrasound impetus (1.0 MHz, W, 3 W/cm^2, 5 min). The intracellular DOX fluorescence was measured at 2 h and 4 h post ultrasound impetus by flow cytometry measurement, where the cells in absence of ultrasonication were employed as the control. In consistent with our speculation, the intracellular level of DOX fluorescence intensity was significant higher for the ultrasound-imposed cells than those without ultrasonication, as evidenced by approximate 1.80-fold higher at 2 h and 1.59-fold higher at 4 h (Figure 3b). In consistent with flow cytometry measurement, CLSM observation also captured a stronger fluorescence signal of intracellular DOX (red) for the ultrasound-treated cells (Figure 3a). Moreover, significant stronger fluorescence signal was observed for the cell s at 4 h relative to that at 2 h, implying consistent release of DOX from P-*oα*-SC/DOX due to the nanostructural rearrangement of P-*oα*-SC/DOX induced by ultrasound-mediated -*oα*- cleavage. Note that substantial DOX was observed in the nuclei of ultrasound-treated cells, which is not observed for the cell in absence of ultrasonication. This observation again approved the functionality of ultrasonication in liberation of DOX as molecular form, which permitted its translocalization across the nucleus membrane and approach its therapeutic targets.

The facilitated drug release and consequent trafficking toward molecular target by ultrasound impetus is believed to contribute enhanced cytotoxic potency to the affected cells. In this regard, the cytotoxicity profiles of P-*oα*-SC in presence and absence of ultrasonication were studied in Hep-G2 cells using MTT assay. Free DOX was employed as a control. As shown in Figure 3c, IC_{50} of free DOX is approximate 2.74 μg/ml, yet the cytotoxicity of P-*oα*-SC was observed to be significant reduced, whose IC_{50} is over 10 μg/ml attributable to the reluctant release of DOX. Nevertheless, IC_{50} of P-*oα*-SC/DOX with aids of ultrasound impetus was calculated to be 2.33 μg/mL, approved the ultrasound-stimulated release to attain ultrasound-controlled cytotoxicity to the internalized cells.

Note that ultrasound itself is not toxic to the cells (Figure 3c), validating the ultrasound stimulus as a superior safe alternative than the other stimuli.

Aside from the targeted cytotoxicity by the proposed ultrasound-based facility, it is also important to verify the minimal cytotoxic activities to the off-target biological structures. To this respect, the cytotoxicity and hemolysis activity of the blank P-*oa*-SC nanoparticulates were investigated to gain the preliminary aspects of the biocompatibilities of the constructed P-*oa*-SC system. Pertaining to the cytotoxic profiles of P-*oa*-SC nanoparticulates, MCF-7 cells, Hela cells, Hep-G2 cells and COS-7 cells were used in an MTT assay. Overall, no significant cytotoxicity was observed for all cell lines treated with P-*oa*-SC despite ultrasound, as evidence by cell viabilities exceeding 90% even P-*oa*-SC at 400 μg/mL to the toxic-sensitive COS-7 cells (Figure S5), indicating the appreciable safety profile of the constructed P-*oa*-SC delivery vehicle.

Hemolysis is acknowledged as an important indicator of cell membrane damage and thus used to estimate the biocompatibility of P-*oa*-SC[32]. At 6 h post incubation, the hemolysis rates of P-*oa*-SC formation were determined to be negligible (below 3% even at a high concentration up to 2 mg/mL), in stark contrast to the hemolysis rates of Tween 80 to be 15.67 % and 71.88 % at the concentration of 0.5 mg /mL and 2 mg/mL) (Figure S6). The results demonstrated that the proposed P-*oa*-SC self-assembly exhibited negligible hemolysis activity, implying its excellent compatibility. Together with the appreciable negligible cytotoxic profile, these results suggested excellent biocompatibility of P-*oa*-SC nanoparticulates, which is believed to be favorable in acquiring high drug bioavailability to the tumors.

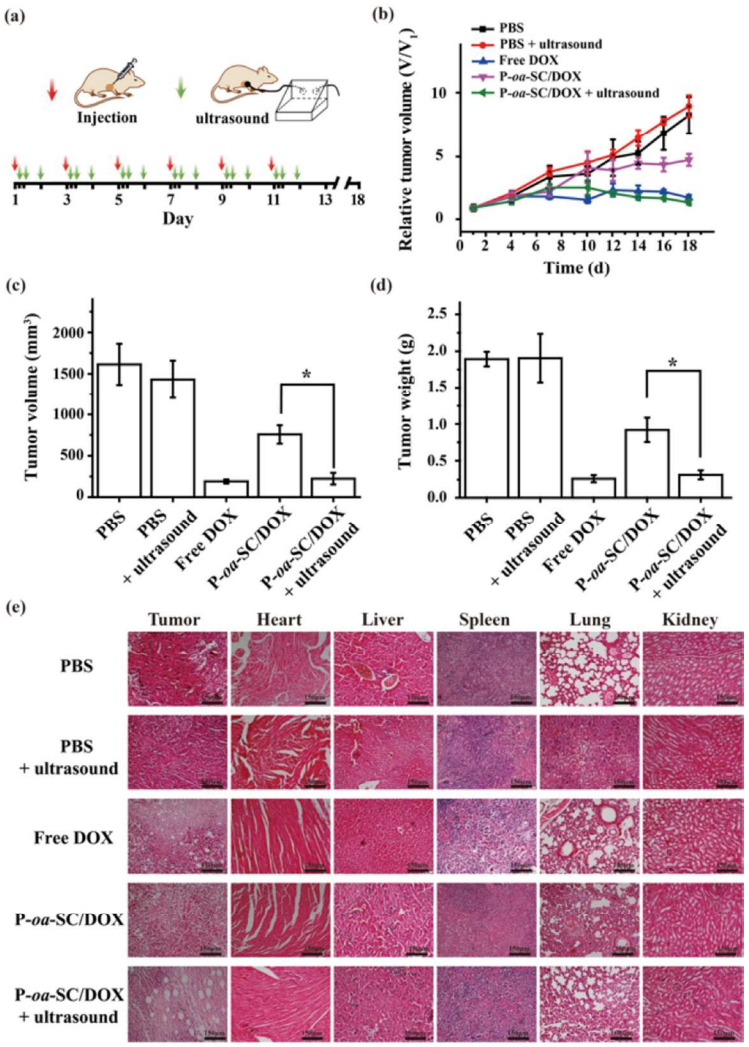

Figure 4. *In vivo* anti-tumor efficacy of P-*oa*-SC/DOX in presence or absence of the tumor-localized ultrasound impetus. a): schematic illustration of tumor-localized ultrasound to promote the cytotoxic potency of administrated P-*oa*-SC/DOX to tumors; b): tumor growth profile; the volumes (c) and weights (d) of anatomical tumor at day 18 post treatment; (e): H&E staining of tumors and major organs at day 18 post treatment. Data were presented as means ± standard error (S.E.). $^{*}p < 0.05$.

Pronounced Anti-Tumor Potency by Virtue of Spatial Ultrasound Impetus to Tumors. In view of the ultrasound-stimulated selective cytotoxicity to the affected cells, we attempted a localized ultrasonication to apply the tumors of 4T1-bearing mice post intratumor administration of P-*oa*-SC/DOX nanoparticles. The anti-tumor efficacy was estimated by measuring the tumor volumes

up to 18 days. As opposed to the limited inhibitory effect on the tumor growth from solely ultrasound treatment (comparable to the PBS control group, approving the safety profile of ultrasound impetus), P-*oa*-SC/DOX exhibited distinctive suppression to the growth of tumors, which is believed to be as result of slow drug diffusion or degradation of the delivery materials eliciting the DOX release from the delivery vehicles to impart chemotherapeutic efficacy. Noteworthy was the potent eradication of solid tumor by P-*oa*-SC/DOX with aids of ultrasound impetus, approving the strategic use of ultrasonication for pursuit of amplified chemotherapeutic potency of the ultrasound-responsive delivery vehicles. Meanwhile, considerable inhibitory efficacy was also obtained from the mice treated by the free DOX, nevertheless, severe systemic toxicity was observed as evidenced by the marked drop in the body weight of the treated mice (Figure S7) and histology analysis of diverse organs (particularly for spleen) by H&E staining (Figure 4e). In contrast, no observable toxicity was confirmed for histology of the major organs (aside from the tumors) from treatment of P-*oa*-SC/DOX. This result approved the appreciable safety profile of P-*oa*-SC/DOX. Pertaining to the histology of the tumors of P-*oa*-SC/DOX-treated group, apparent pycnosis and karyolysis patterns were observed, particular for ultrasound-imposed P-*oa*-SC/DOX group (abundant necrosis and extensive hemorrhagic inflammation). To this end, the ultrasound stimuli-facility in design of DOX delivery vehicles was validated to confer selective amplification of therapeutic potency to the targeted on-demand tumor sites and minimize the potential off-target adverse effect. In view of the wide availability of ultrasound as a spatial precisely localized impetus and the feasibility to attain deep tissue penetration, our elaborated system could be emphasized to develop further to find a broad utility in precision medicine applications.

CONCLUSIONS

In this study, we have successfully tailored an ultrasound-labile -*oa*- linkage between the hydrophobic stearic segments and the hydrophilic pullulan amphiphilic polymer. The developed

pullulan-based amphiphilic polymer was determined to be able to self-assemble with hydrophobic drugs (DOX) into nanoscaled delivery vehicles. The subsequent investigations revealed the proposed pullulan-based delivery nanoparticles (P-*oa*-SC) possessed excellent biocompatibility and particularly presented facile ultrasound-stimulated drug release characters. As a consequence of ultrasound-stimulated cleavage of -*oa*- linkage, the constructed nanostructures have been validated to present ultrasound-accelerated drug delivery profile, which allowed utility of ultrasound as the drug release impetus to acquire selective on-demand chemotherapeutic potency to the targeted cells. Furthermore, dosage of P-*oa*-SC/DOX supplemented with tumor-localized ultrasound exhibited potent anti-tumor efficacy but minimized toxicities to the normal tissues despite the possibility of non-specific distributions of P-*oa*-SC/DOX in the normal tissues. Consequently, the precise spatiotemporal controlled nanomedicine utilizing ultrasound as a convenient external impetus to amplify the cytotoxic potency could serve as an intriguing strategy for maximized inhibition of tumor growth and minimized systemic toxicity.

EXPERIMENTAL SECTION

Materials. Pullulan (M_W = 100 kDa) was purchased from Shandong Zhongqing Biotechnology Company (Zibo, China). 4-chlorobutyryl chloride, pyridine, N, N-dimethylformamide (DMF), 2,2,6,6-HTEMPO, triethylamine (TEA), anhydrous-dichloromethane, stearyl chloride, magnesium sulfate, 2,2'-biopyridine, cuprous bromide, pyrene, 1-methyl-2-pyrrolidinone, dimethyl sulfoxide (DMSO), 3-(4,5-dimethylthiazol-2-yl)-2,5-diphenyltetrazolium bromide (MTT), colchicine, chlorpromazine (CPM) were all obtained from Sigma-Aldrich (St. Louis, USA). Doxorubicin hydrochloride (referred as DOX hereafter) was purchased from Dalian Meilun Biotechnology Co. Ltd. (Dalian, China). All the other chemicals and solvents were purchased from Sigma-Aldrich (St. Louis, USA). The cell lines, including human breast cancer cell (MCF-7), human cervical cancer cell (HeLa) and human hepatoma cell (Hep-G2), mouse mammary tumor cell (4T1) and monkey kidney cell (COS-7), were purchased

from Cell Bank of Shanghai Institute of Biochemistry and Cell Biology (Shanghai, China). Dulbecco's modified Eagle's medium (DMEM) and fetal bovine serum (FBS) were purchased from Hyclone (Logan, MA). Female Bal b/c mice (5 weeks old) were purchased from the animal experiment center of Dalian Medical University (Dalian, China). All animal experimental protocols were established according to the guidelines of the Animal Committee of Dalian University of Technology.

Synthesis and Characterizations of P-*oa*-SC. The synthetic procedure of ultrasound-responsive P-*oa*-SC was illustrated in Scheme 1. In brief, the chloride-functionalized pullulan (P-Cl) was obtained by reaction of 4-chlorobutyryl chloride and pullulan, wherein pullulan (1.62 g, 10 mmol) in 60 mL DMF was titrated with 4-chlorobutyryl chloride (1.72 mL, 15.37 mmol) and small-amount of pyridine. At 36 h post reaction at room temperature, the reaction mixture was poured into 600 mL ethyl alcohol to precipitate P-Cl. The yielded P-Cl was dissolved in 15 mL deionized water and transferred to dialysis (MWCO: 3,500 Da) in deionized water for 5 times. The solid P-Cl product was obtained by lyophilization as white powder. The product was transferred to ^{1}H-NMR measurement for quantification of chloride composition in the yielded P-Cl.

Furthermore, the piperidinyl stearate (OC) was synthesized according to the procedures as previously reported[33]. Briefly, HTEMPO (1.034 g, 6 mmol) and triethylamine (0.83 mL, 6 mmol) were dissolved in 15 mL anhydrous-dichloromethane and stirred for 30 min in ice-water bath prior to reaction. Stearic chloride (1.81 mL, 6 mmol) 10 mL anhydrous-dichloromethane was added to aforementioned dichloromethane solution in argon atmosphere, followed by 30 °C reaction for 24 h. The crude product was subjected to extraction in water to remove unreacted HTEMPO. The organic phase collected and subjected to sequential treatments with magnesium sulfate, filtration over filter paper, evaporation and column chromatography (petroleum ether: ethyl acetate=9:1) to yield OC as dark solid.

Finally, P-*oa*-SC was synthesized based on nitroxide radical coupling reaction according to the procedures as previously reported[34]. In brief, P-Cl (340 mg, n_{Cl} = 0.14 mmol), OC (42.5 mg, 0.1 mmol)

and 2,2'-biopyridine (62.4 mg, 0.4 mmol) were dissolved in 30 mL 1-methyl-2-pyrrolidinone, followed by stirring in argon atmosphere at 25 °C for 30 min with aim of eliminating unfavorable oxygen. Furthermore, cuprous bromide (0.0286 g, 0.2 mmol) was added the aforementioned 1-methyl-2-pyrrolidinone solution and subjected to reaction for 24 h at 40 °C. The crude product of P-*oα*-SC was obtained by precipitation in anhydrous ethanol, followed by dialysis (MWCO: 3500 Da) in deionized water for 5 times. The P-*oα*-SC solid was obtained by lyophilization. The number of SC segments per P-*oα*-SC was estimated based on ^{1}H-NMR measurement (Advance II 400, Bruker, Switzerland).

Preparation and Characterizations of P-*oα*-SC Self-Assembly. P-*oα*-SC self-assembly was prepared according to a dialysis method[10]. Briefly, the synthesized P-*oα*-SC (10 mg) was dissolved in DMSO (3 mL), which was transferred in a dialysis tube (MWCO: 3500 Da) in deionized water or PBS (10 mM, pH 7.4) for 5 times at 4 °C to afford the self-assembly formation of P-*oα*-SC.

A pyrene assay was utilized in pertinent to the critical micelles concentration (CMC) of the synthesized amphiphilic P-*oα*-SC[35]. Herein, a constant concentration of pyrene (6.0×10^{-7} mol/L) was mixed with a class of P-*oα*-SC solution with varied concentrations, ranging from 5×10^{-4} mg/mL to 1 mg/mL). The fluorescence excitation spectra of pyrene (6×10^{-7} mol/L) were recorded (ex: 334 nm, em: 340-450 nm). The index of the fluorescence intensity at 372 nm (I_{372}) and 383 nm (I_{383}) was calculated to infer the behaviors of pyrene molecules trapped into the stearic-aggregated hydrophobic regions of the self-assembled formation.

Furthermore, the particle size and zeta potential of nanoparticles were characterized by dynamic light scattering (DLS, Zetasizer Nano-ZS90, Malvern instruments, UK) measurement. All of the DLS measurements were performed at 25°C. Of note, the concentration of the self-assembly was adjusted at a uniform concentration (1.0 mg/mL) in deionized water or PBS (10 mM, pH 7.4).

The ultrasound-stimulated disassembly behaviors of P-*oα*-SC formation was studied by monitoring the hydrodynamic diameter change under ultrasound treatment. Briefly, P-*oα*-SC

self-assembly (1.0 mg/mL) were placed inside an acoustic power system (Huis bio engineering technology Co. Ltd., City, China) and subjected to ultrasound treatment (1.0 MHz, 9.9 W, 3 W/cm^2, 10 min, 20 min or 30 min) at 37 °C.

Moreover, the aforementioned solution post ultrasound treatment was transferred to Liquid Chromatography Mass Spectrometry measurement (1100HPLC&6130MSD, Agilent, Waters, Santa Clara, CA) measurement to explore evidence of the cleavage of the -*oa*- linkage in P-*oa*-SC.

Preparation and Characterizations of DOX-Loaded P-*oa*-SC/DOX Delivery System. DOX-loaded P-*oa*-SC (P-*oa*-SC/DOX) nanoparticulates were prepared by following a dialysis method as previously reported[17]. In brief, DMSO solution containing P-*oa*-SC (5 mg/mL) and varied concentrations of DOX was transferred to dialysis (MWCO: 3500 Da) in deionized water for 5 times.

DOX Release Behaviors Under Ultrasound Impetus. The DOX release profiles from P-*oa*-SC/DOX formation under ultrasound were characterized to verify the strategical use of -*oa*- linkage for pursuit of ultrasound-stimulated release. In brief, P-*oa*-SC/DOX formation in PBS (10 mM, pH 7.4) were subjected to ultrasound (1.0 MHz, 9.9 W, 3 W/cm^2, 37 °C) for a 10 min, 20 min or 30 min period. Note that the periodic ultrasound schemes alternative to continuous ultrasound were employed: a maximum of 90 s continuous ultrasound followed by 3 min interval (appreciable safety profiles with negligible cytotoxicity confirmed for the periodic ultrasound scheme). The aforementioned solutions were injected into dialysis bags (MWCO: 3500 Da), followed by dialysis in 100 mL PBS (10 mM, pH 7.4) on top of a shaking incubator at 37 °C under dark. At predetermined time intervals, 3 mL of external solution was collected for quantification of DOX by fluorescence measurement (ex: 505 nm, em: 561 nm). Of note, 3 mL of fresh PBS (10 mM, pH 7.4) was fused back to the dialysis phase.

Cytotoxicity. The cytotoxicity of P-*oa*-SC nanoparticle was studied by an MTT assay against Hep-G2 cells, MCF-7 cells, COS-7 cells and Hela cells. In brief, Cells were seeded onto a 96-well plate (10^4 cells/well) and cultured in 100 μL DMEM medium at 37°C, 5% CO_2. At 24 h post incubation, the

cell culture medium was replaced by the fresh one containing varied concentrations of P-*oα*-SC nanoparticle. Following another 48 h incubation, the cell viability was measured by following MTT protocol[36]. Note that the untreated cells were used as the control. Cell viability was expressed as a percentage to the control.

Intracellular Drug Releasing. The intracellular drug releasing profile of nanoparticles was investigated by CLSM (OLYMPUS FV1000, Olympus, Japan) and Flow cytometry (FACS Canto TM, BD, USA). Herein, MCF-7 cells (10^5 cells/well) were seeded onto glass bottom dishes and cultured in DMEM medium supplemented with 10% FBS (37 °C, 5% CO_2). At 24 h post incubation, the cell medium was replaced with fresh one containing P-*oα*-SC/DOX sample. At 30 min post incubation, the cells were washed with PBS and incubated in fresh medium. Furthermore, the cells treated with P-*oα*-SC/DOX sample were either scheduled to ultrasound impetus (1.0 MHz, 9.9 W, 5 min: two circles of 150 s ultrasound treatment with 150 s interval) and additional 1.5 h or 3.5 h incubation or directly incubated in fresh medium for 2 h or 4 h. Prior to CLSM observation, the cells were washed three times with PBS, and stained with Hoechst 33342. The fluorescence images were observed by CLSM (Hoechst 33342: Ex = 405 nm, Em = 460-500 nm; DOX: Ex = 488 nm, Em = 560-600 nm). Aiming for precisely quantification of intracellular fluorescence intensities of DOX with or without ultrasound, the cells were rinsed with PBS for three times and collected by sequential treatments of trypsinization, centrifugation and resuspension in 300 μL PBS. The fluorescence intensity of DOX in each sample was analyzed with PE filter set (Ex: 485 nm, Em: 520-560 nm) by a flow cytometer (BD FACSCanto II, Franklin Lakes, NJ).

***In Vitro* Chemotherapeutic Potency.** The *in vitro* chemotherapeutic potency of P-*oα*-SC/DOX were studied against the cancerous cell lines of Hep-G2 cells and MCF-7 cells by an MTT assay. In brief, Hep-G2 or MCF-7 cells were seeded onto a 96-well plate (10^4 cells/well) and cultured in 100 μL DMEM medium at 37°C, 5% CO_2. At 24 h post incubation, the cell culture medium was replaced by the fresh one containing varied concentrations of P-*oα*-SC/DOX. At 4 h post incubation, the cells

were washed by PBS and incubated in a fresh medium, followed by 5 min ultrasound (1.0 MHz, 9.9 W, …W/cm^2, two circles of 150 s ultrasound treatment with 150 s interval) and additional 24 h incubation. The cell viabilities were measured by MTT method. Note that the untreated cells were used as a control. The Cell viabilities were expressed as a percentage of the control.

***In Vivo* Anti-Tumor Efficacy.** 4T1 cells (2×10^6) in PBS solution (100 μL) were subcutaneously injected into both flanks of female nude Balb/c mice (aged 6-8 weeks). Once the tumor size approaching approximately 50 mm^3, the tumor-bearing mice were randomly assigned into the following five groups (n=3): (1) control (only injected with PBS); (2) PBS with tumor-localized ultrasound impetus (3.0 MHz, 2 W/cm^2, 3 min); (3) free DOX; (4) P-*oa*-SC/DOX without tumor-localized ultrasound; (5) P-*oa*-SC/DOX with tumor-localized ultrasound (3.0 MHz, 2 W/cm^2, 3 min). The dosage of DOX was based on the weight of mice (4 mg/kg). All the mice were subject to intratumor injection every other day and subjected to ultrasound impetus for 3 min at 4, 8 and 24 h post injection. Note that the periodic ultrasound schemes were employed to avoid the potential ultrasound-induced thermal consequences to the tumors: a maximum of 90 s continuous ultrasound followed by a minimum of 180 s interval (appreciable safety profiles without observable cytotoxicity confirmed for the proposed periodic ultrasound scheme in Figure 4b). The therapeutic efficacy was estimated by measuring the tumor volume, body weight in each group every three days in the duration of 18 days. Tumor volume was calculated according to the following equation: tumor volume (cm^3) = length (width)^2/2. Relative tumor volume and relative body weight of mice were calculated as V/V_1, and W/W_1, respectively. (V_1 and W_1 represent the tumor volume and body weight at day 0). The mice were sacrificed and the tumors were collected after treatments at day 18.

***Ex Vivo* Histological Staining.** The 4T1-cell bearing mice were sacrificed at 18 days post dosage. The major functional organs including hearts, livers, spleens, lungs, kidneys, and tumors were dissected and transferred to fixation in a 4% paraformaldehyde solution at room temperature. Furthermore, the treated tissue samples were embedded in paraffin and subjected to section into

5-8 μm thickness. H&E staining (BBC Biochemical, Mount Vernon, WA) was performed for subsequent observation of tissue sections using an IX-83 bright-field/fluorescence microscope (Olympus, Tokyo, Japan).

Statistical Analysis. All the experiments were performed three times unless specifically mentioned and the data were presented as means ± standard deviation (S.D.). Statistical analysis was conducted with the Student's t-test and one-way analysis of variance (ANOVA) analysis by Origin software. The statistical significance was concluded when p value < 0.05 (*) and p value < 0.01 (**).

Supporting Information

The Supporting Information is available free of charge on the ACS Publications website at DOI: Estimation of critical micelles concentration of P-*oa*-SC, colloidal stability of P-*oa*-SC self-assembly, TEM morphologies, cell viabilities of the blank P-*oa*-SC self-assembly, hemolysis activities of P-*oa*-SC self-assembly, and body weight post diverse treatment.

AUTHOR INFORMATION

Corresponding Authors

*E-mail: qixian@dlut.edu.cn

Notes

The authors declare no competing financial interest.

ACKNOWLEDGMENTS

This research was funded by National Natural Science Foundation of China (No. 21376039, U1608222). and the funding support from the Fundamental Research Funds for the Central Universities [No. DUT17RC(3)059].

REFERENCES

(1) Lin, W. (2015) Introduction: nanoparticles in medicine. *Chem. Rev. 115*, 10407–10409.

(2) Davis, M. E., Chen, Z. G., and Shin, D. M. (2008) Nanoparticle therapeutics: an emerging treatment modality for cancer. *Nat. Rev. Drug Discov. 7*, 771–782.

(3) Kamaly, N., Xiao, Z. Y., Valencia, P. M., Radovic-Moreno, A. F., and Farokhzad, O. C. (2012) Targeted polymeric therapeutic nanoparticles: design, development and clinical translation. *Chem. Soc. Rev. 41,* 2971−3010.

(4) Dawidczyk, C. M., Kim, C., Park, J. H., Russell, L. M., Lee, K. H., Pomper, M. G., and Searson, P. C. (2014) State-of-the-art in design rules for drug delivery platforms: lessons learned from FDA-approved nanomedicines. *J. Control. Release 187*, 133–144.

(5) Wang, F., Porter, M., Konstantopoulos, A., Zhang, P., and Cui, H. (2017) Preclinical development of drug delivery systems for paclitaxel-based cancer chemotherapy. *J. Control. Release 267*, 100–118.

(6) Rapoport, N. Physical stimuli-responsive polymeric micelles for anti-cancer drug delivery. (2007) *Prog. Polym. Sci. 32*, 962–990.

(7) Ulbrich, K., Hola, K., Subr, V., Bakandritsos, A., Tucek, J., and Zboril, R. (2016) Targeted drug delivery with polymers and magnetic nanoparticles: covalent and noncovalent approaches, release control, and clinical studies. *Chem. Rev. 116*, 5338–5431.

(8) Huang, G., and Huang, H. (2018) Hyaluronic acid-based biopharmaceutical delivery and tumor-targeted drug delivery system. *J. Control. Release 278*, 122–126.

(9) Koshkaryev, A., Sawant, R., Deshpande, M., and Torchilin, V. (2013) Immunoconjugates and long circulating systems: origins, current state of the art and future directions. *Adv. Drug Deliv. Rev. 65*, 24–35.

(10) Fu, Y, and Kao, W. J. (2010) Drug release kinetics and transport mechanisms of non-degradable and degradable polymeric delivery systems. *Expert Opin. Drug Deliv*. *7*, 429-444.

(11) Modi, S., and Anderson, B. D. (2013) Determination of drug release kinetics from nanoparticles: overcoming pitfalls of the dynamic dialysis method. *Mol. Pharmaceutics 10*, 3076–3089.

(12) Li, Z., Chen, Q., Qi, Y., Liu, Z., Hao, T., Sun, X., Qiao, M., Ma, X., Xu, T., Zhao, X., et al. (2018) Rational design of multifunctional polymeric nanoparticles based on poly(L-histidine) and d-α-Vitamin E Succinate for reversing tumor multidrug resistance. *Biomacromolecules*, *19*, 2595–2609.

(13) Chen, Q., Osada, K., Ge, Z., Uchida, S., Tockary, T. A., Dirisala, A., Matsui, A., Toh, K., Takeda, K. M., Liu, X., et al. (2017) Polyplex micelle installing intracellular self-processing functionalities without free catiomers for safe and efficient systemic gene therapy through tumor vasculature targeting. *Biomaterials 113*, 253–265.

(14) Yang, Y., Yue, C., Han, Y., Zhang, W., He, A., Zhang, C., Yin, T., Zhang, Q., Zhang, J., Yang, Y., et al. (2016) Tumor-responsive small molecule self-assembled nanosystem for simultaneous fluorescence imaging and chemotherapy of lung cancer. *Adv. Funct. Mater. 26*, 8735–8745.

(15) Wang, T., Chen, Q., Lu, H., Li, W., Li, Z., Ma, J., and Gao, H. (2016) Shedding PEG palisade by temporal photostimulation and intracellular reducing milieu for facilitated intracellular trafficking and DNA release. *Bioconj. Chem. 27*, 1949–1957.

(16) Chen, Q., Qi, R., Chen, X., Yang, X., Wu, S., Xiao, H., and Dong, W. (2017) A targeted and stable polymeric nanoformulation enhances systemic delivery of mRNA to tumors. *Mol. Ther. 25*, 92–101.

(17) Wang, X., Wang, J., Bao, Y., Wang, B., Wang, X., and Chen, L. (2014) Novel reduction-sensitive pullulan-based micelles with good hemocompatibility for efficient intracellular doxorubicin delivery. *RSC Adv. 4*, 60064–60074.

(18) Li, F., Chen, C., Yang, X., He, X., Zhao, Z., Li, J., Yu, Y., Yang, X., and Wang, J. (2018) Acetal-linked hyperbranched polyphosphoester nanocarriers loaded with chlorin E6 for pH-activatable photodynamic therapy. *ACS Appl. Mater. Inter. 10*, 21198–21205.

(19) Zhao, H., Hou, B., Tang, Y., Hu, W., Yin, C., Ji, Y., Lu, X., Fan, Q., and Huang, W. (2016) O-nitrobenzyl-alt-(phenylethynyl)benzene copolymer-based nanoaggregates with highly efficient two-photon-triggered degradable properties via a FRET process. *Polym. Chem.* **2016,** *7*, 3117–3125.

(20) Guo, X., Li, D., Yang, G., Shi, C., Tang, Z., Wang, J., and Zhou, S. (2014) Thermo-triggered drug release from actively targeting polymer micelles. *ACS Appl. Mater. Inter. 6*, 8549–8559.

(21) Zhang, H., Xia, H., Wang, J., and Li, Y. (2009) High intensity focused ultrasound-responsive release

behavior of PLA-*b*-PEG copolymer micelles. *J Control. Release 139*, 31–39.

(22) Husseini, G. A., and Pitt, W. G. (2009) Ultrasonic-activated micellar drug delivery for cancer treatment. *J. Pharm. Sci. 98*, 795–811.

(23) Wang, J., Pelletier, M., Zhang, H., Xia, H., and Zhao, Y. (2009) High-frequency ultrasound-responsive block copolymer micelle. *Langmuir 25*, 13201–13205.

(24) Marin, A., Muniruzzaman, M., and Rapoport, N. (2001) Mechanism of the ultrasonic activation of micellar drug delivery. *J. Control. Release 75*, 69–81.

(25) Husseini, G. A., Myrup, G. D., Pitt, W. G., Christensena, D. A., and Rapoport, N. Y. (2000) Factors affecting acoustically triggered release of drugs from polymeric micelles. *J. Control. Release 69*, 43–52.

(26) Paris, J. L., Cabanas, M. V., Manzano, M., and Vallet-Regi, M. A. (2015) Polymer-grafted mesoporous silica nanoparticles as ultrasound-responsive drug carriers. *ACS Nano 9*, 11023–11033.

(27) Chen, L., Wang, X., Ji, F., Bao, Y., Wang, J., Wang, X., Guo, L., and Li, Y. (2015) New bifunctional-pullulan-based micelles with good biocompatibility for efficient co-delivery of cancer-suppressing p53 gene and doxorubicin to cancer cells. *RSC Adv. 5*, 94719–94731.

(28) Liu, Z., Jiao, Y., Wang, Y., Zhou, C., and Zhang, Z. (2008) Polysaccharides-based nanoparticles as drug delivery systems. *Adv. Drug Deliver. Rev. 60*, 1650–1662.

(29) Prajapati, V. D., Jani, G. K., and Khanda, S. M. (2013) Pullulan: an exopolysaccharide and its various applications. *Carbohydr. Polym. 95*, 540–549

(30) Bae, B. C., and Na, K. (2010) Self-quenching polysaccharide-based nanogels of pullulan/folate-photosensitizer conjugates for photodynamic therapy. *Biomaterials 31*, 6325–6335.

(31) Sirsi, S. R., and Borden, M. A. (2014) Sate-of-the-art materials for ultrasound-triggered drug delivery. *Adv. Drug Delivery Rev. 72*, 3–14.

(32) Zhang, M. K., Wang, X. G., Zhu, J. Y., Liu, M. D., Li, C. X., Feng, J., and Zhang, X. Z. (2018) Double-targeting explosible nanofirework for tumor ignition to guide tumor-depth photothermal therapy. *Small 14*, 180–292.

(33) Wunderlich, W., Clauss, M., Roth., and Fuso, F. Use of 2,2,6,6 tetraalkylpiperidine-N-oxyl radicals having long alkyl chains as polymerization regulators. U.S. Patent 6,569,940, May 27, **2003**.

(34) Lin, W., Huang, B., Fu, Q., Wang, G., and Huang, J. (2010) Investigation of nitroxide radical coupling reaction in wide temperature range and different catalyst system. *J. Polym. Sci. Pol. Chem. 48*, 2991–2999.

(35) Xu, Y., Wang, S., Chan, H. F., Liu, Y., Li, H., He, C., Li, Z., and Chen, M. (2017) Triphenylphosphonium-modified poly(ethylene glycol)-poly(epsilon-caprolactone) micelles for mitochondria-targeted gambogic acid delivery. *Int. J. Pharm. 522*, 21–33.

(36) Zheng, F., Zhang, P., Xi, Y., Chen, J., Li, L., and Zhu, J. (2015) Aptamer/graphene quantum dots nanocomposite capped fluorescent mesoporous silica nanoparticles for intracellular drug delivery and real-time monitoring of drug release. *Anal. Chem. 87*, 11739–11745.

TOC

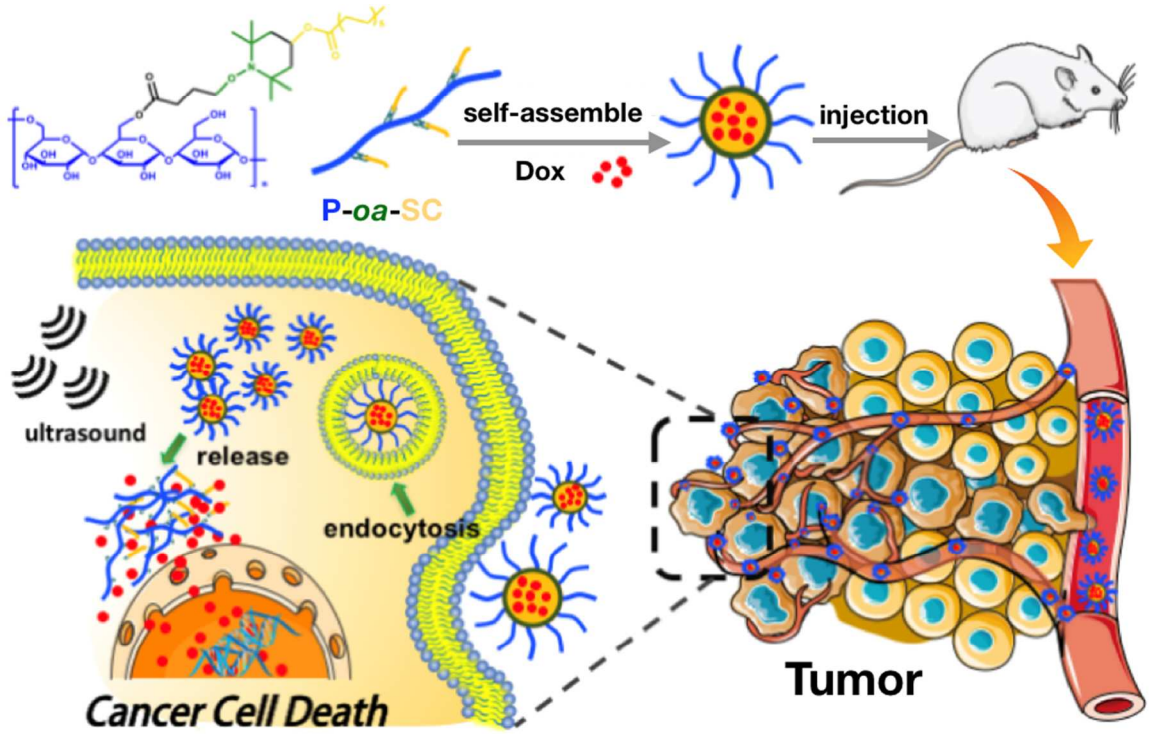
self-assemble
Dox
injection
P-oa-SC
ultrasound
release
endocytosis
Cancer Cell Death
Tumor